Effect of temperature variation on the full-range behavior of FRP-to-concrete bonded joints

W.Y. Gao[1], J.G. Teng[2] and Jian-Guo Dai[3]

Abstract: Service temperature variations (thermal loadings) may significantly affect the behavior of the bond between externally bonded fiber reinforced polymer (FRP) and concrete. This paper presents an analytical solution for the full-range deformation process of FRP-to-concrete bonded joints under combined thermal and mechanical loadings. The solution is based on a bilinear bond-slip model and leads to closed-form expressions. The validity of the solution is demonstrated through comparisons with both experimental results and finite element predictions. Numerical results from the solution are presented to illustrate the effect of thermal loading on the interfacial shear stress and slip distributions as well as the global load-displacement response. It is shown that, provided the material properties are not affected by temperature variations, a temperature rise increases the ultimate load while a temperature reduction decreases the ultimate load; the latter can have serious implications for the safety of the strengthened structure. While the solution is developed with particular reference to FRP-to-concrete bonded joints, it is also applicable to similar bonded joints made of other materials (e.g. FRP-to-steel bonded joints). A useful function of the closed-form solution lies in the interpretation of pull test results: the solution allows the effect of thermal stresses to be isolated from the effect of property changes of the bondline in obtaining bond-slip responses from pull tests.

Keywords: Fiber reinforced polymer (FRP); Concrete; Strengthening; Interfaces; Temperature variations; Debonding; Thermal stresses.

Introduction

In reinforced concrete (RC) structures strengthened with externally bonded fiber reinforced polymer (FRP) reinforcement, the bond behavior between FRP and concrete often controls the load-carrying capacity of the strengthened structure (Teng et al. 2002; Hollaway and Teng 2008). As a result, many studies have been conducted on the bond behavior of FRP-to-concrete interfaces (e.g. Taljsten 1996; Chajes et al. 1996; Yuan et al. 2000; Brosens 2001; Chen and Teng 2001; De Lorenzis et al. 2001; Nakaba et al. 2001; Wu et al. 2002; Dai et al. 2005, 2006; Lu et al. 2005a, 2005b; Yao et al. 2005; Ferracuti et al. 2007; Wang 2007; Achintha 2009; Zhou et al. 2010; Cornetti and Carpinteri 2011). In particular, the single-lap pull test (Fig. 1) (or a double-lap pull test which can be seen as two single-lap pull tests being conducted simultaneously) has been widely used to study the ultimate load (i.e. the bond strength or the debonding load) of FRP-to-concrete bonded joints and the local bond-slip behavior of the FRP-to-concrete interface (e.g. Chajes et al. 1996; Brosens 2001; De Lorenzis et al. 2001; Nakaba et al. 2001; Dai et al. 2005; Yao et al. 2005).

[1] PhD Student, Department of Civil and Structural Engineering, The Hong Kong Polytechnic University, Hong Kong, China.
[2] Chair Professor of Structural Engineering (Corresponding author), Department of Civil and Structural Engineering, The Hong Kong Polytechnic University, Hong Kong, China. Tel: (852) 2766 6012; Fax: (852) 2766 1354; E-mail: cejgteng@polyu.edu.hk.
[3] Assistant Professor, Department of Civil and Structural Engineering, The Hong Kong Polytechnic University, Hong Kong, China.

FRP-strengthened RC structures in service are likely to experience significant temperature variations (e.g. seasonal ambient temperature changes and exposure to fire) and such variations can have a significant effect on the bond performance of FRP-to-concrete interfaces. To understand the bond behavior of FRP-to-concrete interfaces exposed to different temperature variations, the pull test has also been used (e.g. Blontrock 2003; Wu et al. 2005; Klamer 2006, 2009; Leone et al. 2009). Results from such tests reflect directly the combined effects of a number of factors including temperature-induced interfacial stresses and temperature-induced property changes in the bondline (the adhesive and the adjacent parts of the adherends) as well as the adherends if the temperature becomes sufficiently high. A key purpose of such pull tests is to determine the bond-slip curve of the interface at a specific temperature variation, for which the effect of thermal interfacial stresses needs to be isolated from the effect of temperature-induced material property changes, as only the latter should be included in a bond-slip model for use in a theoretical model for FRP-strengthened RC structures subjected to temperature variations. This issue has received little attention and indeed in some existing studies, these thermal stresses were simply ignored in interpreting pull test results (e.g. Wu et al. 2005; Leone et al. 2009).

More recently, Rabinovitch (2010) employed linear elastic fracture mechanics (LEFM) and a high-order interfacial stress analysis to study the effect of temperature variation on debonding in FRP-strengthened concrete members. His analysis is incapable of predicting the full-range nonlinear behavior of the bonded joint. Indeed, given the importance of the softening behavior of the bonded interface after attaining the peak bond stress, an LEFM approach is in general inadequate. This paper presents a theoretical study on the full-range behavior of FRP-to-concrete bonded joints at a specific temperature variation from the reference ambient temperature at installation (referred to as the reference temperature hereafter). An analytical solution, which is an extension of the existing analytical solution of Yuan et al. (2004) for mechanical loading only, is first presented. The validity of the analytical solution is demonstrated through comparisons with the limited available experimental results as well as results from a finite element (FE) model. The effects of temperature variations on the load-displacement response, the ultimate load, the interfacial shear stress distribution and the interfacial slip distribution are all examined in the paper. Finally, the elimination of the thermal stress effect in the determination of the interfacial fracture energy from pull tests at a temperature variation is examined.

Analytical solution

Assumptions and notation

Fig. 1 shows the theoretical idealization of a single-lap bonded joint where both adherends are assumed to experience only membrane deformation. Moreover, it is assumed that the width and thickness of each of the three components (plate, adhesive layer and concrete prism) are constant in the longitudinal direction. In such a simplified theoretical model, the adhesive layer (representing the interface or the bondline whose deformation represents the deformation of the actual adhesive layer and that of the adjacent parts of the two adherends) is subjected to shear deformation, so that mode II interfacial fracture is the failure mode. This theoretical model is a close approximation of the behavior of a real bonded

joint (Yuan et al. 2004; Teng et al. 2006; Chen et al. 2007). In addition, it is assumed that the interface is still within the linear elastic range of behavior and the properties of the adherends are not affected during the imposition of the thermal loading; these two assumptions means that the degree of temperature variation needs to be appropriately limited. The applicability of the solution to bonded joints whose adherends have experienced temperature-induced property degradations is discussed later in this paper.

In Fig. 1, b_p, t_p and L are the thickness, width and bond length of the FRP plate, respectively, while b_c and t_c are the width and thickness of the concrete prism, respectively. The elastic moduli of the plate and the concrete are E_p and E_c, respectively. For convenience of presentation, the left end of the plate (x=0) is referred to as the free end and the right end (x= L) the loaded end hereafter.

Governing equations

Based on the above assumptions, the horizontal equilibrium consideration of the FRP plate and of the overall joint cross-section leads to the following equations:

$$\frac{d\sigma_p}{dx} - \frac{\tau}{t_p} = 0 \tag{1}$$

$$\sigma_p t_p b_p + \sigma_c t_c b_c = 0 \tag{2}$$

where τ is the shear stress in the adhesive layer (the interfacial shear stress), σ_p is the axial stress in the FRP plate and σ_c is the axial stress in the concrete prism. The constitutive equations for the adhesive layer and the two adherends are described by

$$\tau = f(\delta) \tag{3}$$

$$\sigma_p = E_p(\frac{du_p}{dx} - \alpha_p \Delta T) \tag{4}$$

$$\sigma_c = E_c(\frac{du_c}{dx} - \alpha_c \Delta T) \tag{5}$$

where u_p and u_c are the longitudinal displacements of the FRP plate and the concrete, respectively; α_p and α_c are the coefficients of thermal expansion of the FRP plate and the concrete, respectively; and ΔT is the service temperature variation (thermal loading). The interfacial slip δ is defined as the relative displacement between the two adherends; that is

$$\delta = u_p - u_c \tag{6}$$

From Eqs. 1-6, the following second-order differential equation can be derived:

$$\frac{\mathrm{d}^2\delta}{\mathrm{dx}^2} - \frac{2G_f}{\tau_f^2}\,\lambda^2\, f(\delta) = 0 \tag{7}$$

where

$$\lambda^2 = \frac{\tau_f^2}{2G_f}\left(\frac{1}{E_p t_p} + \frac{b_p}{E_c t_c b_c}\right) \tag{8}$$

In Eqs. 7 and 8, τ_f is the local bond strength (i.e. the maximum shear stress on the bond-slip curve) and G_f is the interfacial fracture energy (the area underneath the interfacial bond-slip curve). Substituting Eq. 6 into Eqs. 2, 4 and 5 yields

$$\sigma_p = \frac{\tau_f^2}{2G_f t_p \lambda^2}\left[\frac{d\delta}{dx} - (\alpha_p - \alpha_c)\Delta T\right] \tag{9}$$

Bond-slip model

A bilinear bond-slip model has been widely used to study the bond behavior of FRP-to-concrete bonded joints (e.g. Yuan et al. 2004) as it closely reflects the actual bond-slip response (Lu et al. 2005a). Such a bilinear model is also adopted in the present study. As shown in Fig. 2, the bilinear bond-slip relationship consists of two segments: an initial linear elastic segment where the bond shear stress increases linearly with the interfacial slip until it reaches the peak stress τ_f (the corresponding slip is denoted by δ_1) and a softening segment where the shear stress reduces with the interfacial slip until it becomes zero (the corresponding slip is denoted by δ_f). Note that the same shape is assumed for the bond-slip curve for shear stresses and slips in the opposite direction, but only the curve for positive values of δ is shown in Fig. 2. This bond-slip model (Fig. 2) is described by the following equation:

$$f(\delta) = \begin{cases} \frac{\tau_f}{\delta_1}\,\delta & \text{when } 0 < \delta \le \delta_1 \\ \frac{\tau_f}{\delta_f - \delta_1}(\delta_f - \delta) & \text{when } \delta_1 < \delta \le \delta_f \\ 0 & \text{when } \delta > \delta_f \end{cases} \tag{10}$$

For the present analytical solution, it is assumed that the bond-slip law is fully reversible if slip reversals occur during the deformation process. The implications of this assumption are further discussed later in the paper.

Stages of the debonding process

With the bond-slip model defined above and following the approach of Yuan et al. (2004), the governing equation (Eq. 7) can be solved to find the interfacial shear stress distribution and interfacial slip distribution along the interface and the load-displacement response of the bonded joint under combined thermal and mechanical loadings.

For a bond-slip model as shown in Fig. 2, the entire deformation process can be divided into four stages (Yuan et al. 2004): (1) the elastic stage (Stage I), during which the load P is small and the interfacial shear stress stays below τ_f; (2) the elastic-softening stage (Stage II),

during which the shear slip at the loaded end has exceeded δ_1 but is smaller than δ_f; (3) the elastic-softening-debonding stage (Stage III), during which the interfacial slip at the loaded end has exceeded the separation slip δ_f and the shear stress there has reduced to zero; during this stage, interfacial debonding initiates at the loaded end and propagates along the interface; and (4) the softening-debonding stage (Stage IV), during which the elastic zone has disappeared as a result of propagation of debonding. For a bonded joint under mechanical load only, these stages are illustrated using the interfacial shear stress and slip distributions as well as the load-displacement response obtainable from Yuan et al.'s (2004) solution in Fig. 3; these results are for plate and concrete material properties from Klamer's (2006) tests and a bond-slip curve as described in Section 3.1. For a clearer presentation, the interfacial shear stresses and slips in Fig. 3 are normalized by τ_f and δ_f, respectively. The results shown in Fig. 3 also provide the reference point for the solution presented below.

Elastic stage (Stage I)

During the elastic stage (Figs. 3a), the bond-slip curve is given by the first expression of Eq. 10. Substituting Eq. 10 into Eq. 7, the following differential equation is obtained:

$$\frac{\mathrm{d}^2\delta}{\mathrm{dx}^2} - \lambda_1^2\,\delta = 0 \tag{11}$$

where

$$\lambda_1^2 = \frac{2G_f}{\delta_1\tau_f}\,\lambda^2 = \frac{\tau_f}{\delta_1}\left(\frac{1}{\mathrm{E_p}t_p} + \frac{b_p}{\mathrm{E_c}t_c b_c}\right) \tag{12}$$

Substituting the boundary conditions (σ_p= 0 at x= 0; σ_p= $\frac{P}{b_p t_p}$ at x= L) into Eq. 11, the expressions for the interfacial slip, the interfacial shear stress and the axial stress in the plate are obtained:

$$\delta = \left\{\frac{P\,\lambda_1\,\delta_1}{b_p\tau_f} + \frac{(\alpha_p-\alpha_c)\Delta T[1-\cosh(\lambda_1 L)]}{\lambda_1}\right\}\cdot\frac{\cosh(\lambda_1 x)}{\sinh(\lambda_1 L)} + \frac{(\alpha_p-\alpha_c)\Delta T}{\lambda_1}\cdot\sinh(\lambda_1 x) \tag{13}$$

$$\tau = \frac{\tau_f}{\delta_1}\left\{\left[\frac{P\,\lambda_1\,\delta_1}{b_p\tau_f} + \frac{(\alpha_p-\alpha_c)\Delta T[1-\cosh(\lambda_1 L)]}{\lambda_1}\right]\cdot\frac{\cosh(\lambda_1 x)}{\sinh(\lambda_1 L)} + \frac{(\alpha_p-\alpha_c)\Delta T}{\lambda_1}\cdot\sinh(\lambda_1 x)\right\} \tag{14}$$

$$\sigma_p = \frac{\tau_f}{\delta_1 t_p \lambda_1^2}\left\{\left[\frac{P\lambda_1^2\delta_1}{b_p\tau_f} + (\alpha_p-\alpha_c)\Delta T[1-\cosh(\lambda_1 L)]\right]\cdot\frac{\sinh(\lambda_1 x)}{\sinh(\lambda_1 L)} + (\alpha_p-\alpha_c)\Delta T\cdot \cosh(\lambda_1 x) - (\alpha_p-\alpha_c)\Delta T\right\} \tag{15}$$

The slip at the loaded end (i.e. the value of δ at x=L) is also referred to as the displacement of the bonded joint and is denoted by Δ. Based on this definition, the load-displacement relationship is given by:

$$P = \Delta \times \left\{\left[1 - \frac{(\alpha_p - \alpha_c)\Delta T}{\lambda_1 \Delta} \cdot \sinh(\lambda_1 L)\right] - \frac{(\alpha_p - \alpha_c)\Delta T[1 - \cosh(\lambda_1 L)]}{\lambda_1 \Delta \cdot \tanh(\lambda_1 L)}\right\} \cdot \frac{b_p \tau_f}{\lambda_1 \delta_1} \cdot \tanh(\lambda_1 L) \quad (16)$$

The initial displacement Δ_0 due to the temperature variation can be calculated as (i.e. P= 0 and x= L in Eq. 13):

$$\Delta_0 = \frac{(\alpha_p - \alpha_c)\Delta T[1 - \cosh(\lambda_1 L)]}{\lambda_1} \cdot \operatorname{ctanh}(\lambda_1 L) + \frac{(\alpha_p - \alpha_c)\Delta T}{\lambda_1} \cdot \sinh(\lambda_1 L) \quad (17)$$

At the end of the elastic stage, the interfacial shear stress reaches τ_f with a slip δ_1 at the loaded end. Substituting $\Delta = \delta_1$ at x=L into Eq. 13 leads to the load at the initiation of interfacial softening (the beginning of the elastic-softening stage):

$$P_e = \left\{\left[1 - \frac{(\alpha_p - \alpha_c)\Delta T}{\lambda_1 \delta_1} \cdot \sinh(\lambda_1 L)\right] - \frac{(\alpha_p - \alpha_c)\Delta T[1 - \cosh(\lambda_1 L)]}{\lambda_1 \delta_1 \cdot \tanh(\lambda_1 L)}\right\} \cdot \frac{b_p \tau_f}{\lambda_1} \cdot \tanh(\lambda_1 L) \quad (18)$$

For an infinite bond length, Eq. 18 reduces to

$$P_e = \left[1 - \frac{(\alpha_p - \alpha_c)\Delta T}{\lambda_1 \delta_1}\right] \cdot \frac{\tau_f b_p}{\lambda_1} \quad (19)$$

Elastic-softening stage (Stage II)

When the loaded end slip first exceeds δ_1, the free end slip is still less than δ_1, so the right part of the interface (i.e. the part near the loaded end) is now in a softening state while the left part of the interface (i.e. the part near the free end) is still in the linear elastic state (Figs. 3a). As the load P further increases, the length of the softening zone (denoted as a) also increases. Substituting the relevant relationships given by Eq. 10 into Eq. 7, the following governing equations for the elastic-softening stage can be obtained:

$$\frac{\mathrm{d}^2\delta}{\mathrm{dx}^2} - \lambda_1^2 \delta = 0 \qquad \text{for } 0 \le \delta \le \delta_1 \quad (20)$$

$$\frac{\mathrm{d}^2\delta}{\mathrm{dx}^2} + \lambda_2^2 \delta = \lambda_2^2 \delta_f \qquad \text{for } \delta_1 < \delta \le \delta_f \quad (21)$$

where

$$\lambda_2^2 = \frac{2G_f}{(\delta_f - \delta_1)\tau_f} \lambda^2 = \frac{\tau_f}{(\delta_f - \delta_1)} \left(\frac{1}{\mathrm{E_p} t_p} + \frac{b_p}{\mathrm{E_c} t_c b_c}\right) \quad (22)$$

The boundary conditions are defined as:

$$\sigma_p = 0 \text{ at } x = 0 \quad (23)$$

$$\sigma_p \text{ is continuous at } x = L - a \tag{24}$$

$$\tau = \tau_f \text{ at } x = L - a \tag{25}$$

$$\sigma_p = \frac{P}{b_p t_p} \text{ at } x = L \tag{26}$$

Making use of the boundary conditions, the solutions in the elastic zone ($0 \leq x \leq L - a$, $0 \leq \delta \leq \delta_1$) have the same form as Eqs. 13-15:

$$\delta = \frac{\lambda_1\delta_1 - (\alpha_p - \alpha_c)\Delta T \sinh(\lambda_1(L-a))}{\lambda_1 \cosh(\lambda_1(L-a))} \cdot \cosh(\lambda_1 x) + \frac{(\alpha_p - \alpha_c)\Delta T}{\lambda_1} \cdot \sinh(\lambda_1 x) \tag{27}$$

$$\tau = \frac{\tau_f}{\delta_1}\left\{\frac{\lambda_1\delta_1 - (\alpha_p - \alpha_c)\Delta T \sinh(\lambda_1(L-a))}{\lambda_1 \cosh(\lambda_1(L-a))} \cdot \cosh(\lambda_1 x) + \frac{(\alpha_p - \alpha_c)\Delta T}{\lambda_1} \cdot \sinh(\lambda_1 x)\right\} \tag{28}$$

$$\sigma_p = \frac{\tau_f}{\lambda_1^2 t_p \delta_1}\left\{\frac{\lambda_1\delta_1 - (\alpha_p - \alpha_c)\Delta T \sinh(\lambda_1(L-a))}{\cosh(\lambda_1(L-a))} \cdot \sinh(\lambda_1 x) + [\cosh(\lambda_1 x) - 1](\alpha_p - \alpha_c)\Delta T\right\} \tag{29}$$

In the softening zone ($L - a \leq x \leq L,\ \delta_1 < \delta \leq \delta_f$), the interfacial slip, the interfacial shear stress and the axial stress in the FRP plate are given by:

$$\delta = \delta_f + \frac{1}{\lambda_2}\left[\lambda_1\delta_1 \tanh(\lambda_1(L-a)) + \frac{(\alpha_p - \alpha_c)\Delta T}{\cosh(\lambda_1(L-a))}\right] \cdot \sin(\lambda_2(x - L + a)) + (\delta_1 - \delta_f) \cdot \cos(\lambda_2(x - L + a)) \tag{30}$$

$$\tau = -\tau_f\left\{\frac{1}{\lambda_2(\delta_f - \delta_1)}\left[\lambda_1\delta_1 \cdot \tanh(\lambda_1(L-a)) + \frac{(\alpha_p - \alpha_c)\Delta T}{\cosh(\lambda_1(L-a))}\right] \cdot \sin(\lambda_2(x - L + a)) - \cos(\lambda_2(x - L + a))\right\} \tag{31}$$

$$\sigma_p = -\frac{\tau_f}{\lambda_1^2 t_p \delta_1}(\alpha_p - \alpha_c)\Delta T + \frac{\tau_f}{t_p}\frac{1}{\lambda_1^2\,\delta_1}\left[\lambda_1\delta_1 \tanh(\lambda_1(L-a)) + \frac{(\alpha_p - \alpha_c)\Delta T}{\cosh(\lambda_1(L-a))}\right] \cdot \cos(\lambda_2(x - L + a)) + \frac{\tau_f}{t_p\,\lambda_2} \cdot \sin(\lambda_2(x - L + a)) \tag{32}$$

Substituting the boundary condition $\sigma_p = \frac{P}{b_p t_p}$ at the loaded end ($x = L$) into Eq. 32 yields

$$P = -\frac{b_p\tau_f}{\lambda_1^2\delta_1}(\alpha_p - \alpha_c)\Delta T + \frac{b_p\tau_f}{\lambda_1^2\,\delta_1}\left[\lambda_1\delta_1 \tanh(\lambda_1(L-a)) + \frac{(\alpha_p - \alpha_c)\Delta T}{\cosh(\lambda_1(L-a))}\right] \cdot \cos(\lambda_2 a)$$

$$+\frac{b_p\tau_f}{\lambda_2}\cdot\sin(\lambda_2 a) \tag{33}$$

and the displacement Δ at the loaded end can be found from Eq. 30 (i.e. x= L) to be

$$\Delta=\delta_f+\frac{1}{\lambda_2}\left[\lambda_1\delta_1\tanh\big(\lambda_1(L-a)\big)+\frac{(\alpha_p-\alpha_c)\Delta T}{\cosh(\lambda_1(L-a))}\right]\cdot\sin(\lambda_2 a)+(\delta_1-\delta_f)\cdot\cos(\lambda_2 a) \tag{34}$$

Eqs. 33 and 34 can be used to predict the load-displacement relationship for the elastic-softening stage by varying the value of a.

Elastic-softening-debonding stage (Stage III)

At the end of Stage II (Fig. 3a), the slip at the loaded end Δ reaches δ_f, indicating the initiation of debonding at the loaded end. The corresponding value of a is its maximum possible value (denoted by a_d) and is determined using the following equation which is obtained from Eq. 34:

$$\frac{1}{\lambda_2}\left[\lambda_1\delta_1\tanh\big(\lambda_1(L-a_d)\big)+\frac{(\alpha_p-\alpha_c)\Delta T}{\cosh(\lambda_1(L-a_d))}\right]\cdot\sin(\lambda_2 a_d)+(\delta_1-\delta_f)\cdot\cos(\lambda_2 a_d)=0 \tag{35}$$

Substituting Eq. 35 into Eq. 33 yields

$$P_u=\frac{b_p\tau_f}{\lambda_2}\cdot\frac{\delta_f}{\delta_f-\delta_1}\cdot\sin(\lambda_2 a_d)-\frac{b_p\tau_f}{\lambda_1^2\delta_1}\big(\alpha_p-\alpha_c\big)\Delta T \tag{36}$$

For an infinite bond length, Eq. 35 reduces to

$$a_d=\frac{1}{\lambda_2}\arctan\left\{\frac{\lambda_1}{\lambda_2}\right\} \tag{37}$$

and Eq. 36 reduces to

$$P_u=\frac{b_p\tau_f}{\lambda}-\frac{b_p\tau_f}{\lambda_1^2\delta_1}\big(\alpha_p-\alpha_c\big)\Delta T \tag{38}$$

As the debonding crack propagates, the location of the peak shear stress τ_f moves away from the loaded end towards the free end, and as a result, the total length of the intact interface reduces and the pull load starts to decrease (unless the bond length is infinitely long for which the pull load remains constant during crack propagation). Assuming that the length of the debonded interface is d (see Fig. 3a), the equations derived for Stage II for the interfacial slip, the interfacial shear stress, the FRP plate axial stress (Eqs. 27-32) and the pull load (Eq. 33) are still valid for Stage III if L is replaced by (L-d). The displacement can be evaluated with the consideration of thermal deformation in the debonded zone and is given by the following equation:

$$\Delta = \delta_f + \frac{P}{b_p}\left(\frac{1}{\mathrm{E_p}t_p} + \frac{b_p}{\mathrm{E_c}t_c b_c}\right) d + \left(\alpha_p - \alpha_c\right)\Delta T d \tag{39}$$

Softening-debonding stage (Stage IV)

The softening-debonding stage initiates when $L - d = a_u$ (Fig. 3a), and it is governed by Eq. 21 with the following boundary conditions:

$$\sigma_p = 0 \text{ at } x = 0 \tag{40}$$

$$\delta = \delta_f \text{ and } \sigma_p = \frac{P}{b_p t_p} \text{ at } x = a_u \tag{41}$$

The following solution can thus be found for $0 \le x \le a_u$

$$\delta = \delta_f + A\sin(\lambda_2 x) + B\cos(\lambda_2 x) \tag{42}$$

$$\tau = \frac{\tau_f}{\delta_f - \delta_1} \cdot (\delta_f - \delta) \tag{43}$$

$$\sigma_p = \frac{\tau_f}{\lambda_2^2 t_p (\delta_f - \delta_1)}\left[A\lambda_2\cos(\lambda_2 x) - B\lambda_2 \sin(\lambda_2 x) - \left(\alpha_p - \alpha_c\right)\Delta T\right] \tag{44}$$

where

$$A = \frac{1}{\lambda_2}\left(\alpha_p - \alpha_c\right)\Delta T \tag{45}$$

$$B = -\left[\frac{(\alpha_p - \alpha_c)\Delta T}{\lambda_2} + \frac{P\lambda_2(\delta_f - \delta_1)}{b_p \tau_f}\right]\sin(\lambda_2 a_u) \tag{46}$$

$$a_u = \frac{1}{\lambda_2} \cdot \arccos\left[\frac{\frac{1}{\lambda_2}(\alpha_p - \alpha_c)\Delta T}{\frac{1}{\lambda_2}(\alpha_p - \alpha_c)\Delta T + \frac{P\lambda_2(\delta_f - \delta_1)}{b_p \tau_f}}\right] \tag{47}$$

Eq. 47 indicates that as the pull load increases, the softening zone length a_u (over which interfacial shear stresses exist) increases if $\Delta T > 0$ but decreases if $\Delta T < 0$. The load -displacement relationship can be obtained by replacing d with $(L - a_u)$ in Eq. 39:

$$\Delta = \delta_f + \frac{P}{b_p}\left(\frac{1}{\mathrm{E_p}t_p} + \frac{b_p}{\mathrm{E_c}t_c b_c}\right)(L - a_u) + \left(\alpha_p - \alpha_c\right)\Delta T(L - a_u) \tag{48}$$

During this softening-debonding stage, if there is no thermal loading, Eq. 47 indicates that a_u is a constant (Yuan et al. 2004; Fig. 3b) and the slip at the loaded end reduces linearly with the load as indicated by Eq. 48. At the same time, the slip at the free-end

increases as the load reduces and when this slip reaches δ_f, the slip values everywhere along the interface are equal to δ_f (Fig. 3b), which means that the entire interface has debonded and the pull load is now zero. Note that during the entire deformation process, although slip reversals occur near the loaded end, these reversals are never large enough to reduce a slip value larger than δ_f to below δ_f; that is, slip reversals do not have any implication for the assumed bond-slip model. However, when thermal loading exists, the response of the bonded joint becomes more complicated during this stage and depends on whether $\Delta T > 0$ or $\Delta T < 0$.

When $\Delta T < 0$, the softening zone length a_u with active shear stresses becomes shorter than that of the reference temperature case (Fig. 11d). Similar to the reference temperature case, when the slip at the free end reaches δ_f, the slip values everywhere along the entire interface are larger than δ_f (Fig. 11d) (hence the softening zone length a_u reduces to zero) and the pull load becomes zero.

When $\Delta T > 0$, the softening zone length a_u becomes greater than that of the reference temperature case (Fig. 10d) and before the entire interface reaches debonding, parts of the interface have experienced slip reversals to values below δ_f (Figs. 10d and 10e). Due to these slip reversals, the analytical solution depends on the assumed behavior of the bond-slip model during such slip reversals. For simplicity of solution, it is assumed for the present solution that the bond-slip relationship is fully reversible when local slip reversals occur. The effect of assuming a different unloading path for slip reversals is examined later using an FE model (Figs. 10d and 10e). Under the assumption of a fully reversible bond-slip law, the softening zone expands towards the loaded end during this stage, due to the assumed ability of the debonded interface to regain resistance. This expansion ends when the slip at the free end reaches δ_f and the softening zone length a_u reaches its maximum possible value a_{umax}. (Fig. 10d). Afterwards, the boundary condition described by Eq. 41 is no longer valid. Different from the case of $\Delta T < 0$, the fact that the free-end slip reaches δ_f does not mean that interfacial slip values at other locations of the interface are larger than δ_f . After the free-end slip reaches δ_f (referred to as Stage IV'), the boundary condition at the free end becomes:

$$\tau = 0 \text{ and } \sigma_p = 0 \text{ at } x = 0 \tag{49}$$

Substituting Eq. 49 into the governing equation (i.e. Eq. 21) leads to a solution that has the same form as Eqs. 42-44 with the parameters A and B being given by

$$A = \frac{1}{\lambda_2}(\alpha_p - \alpha_c)\Delta T \tag{50}$$

$$B = 0 \tag{51}$$

During Stage IV', the bond length with active bond stresses (i.e. defined as a_u') decreases from a_{umax} and the load-displacement response can be obtained from the following equations:

$$P = \frac{\tau_f b_p}{\lambda_2^2(\delta_f - \delta_1)}\left[(\alpha_p - \alpha_c)\Delta T \cos(\lambda_2 a_u') - (\alpha_p - \alpha_c)\Delta T\right] \quad (52)$$

$$\Delta = \delta_f + \frac{1}{\lambda_2}(\alpha_p - \alpha_c)\Delta T \sin(\lambda_2 a_u') \quad (53)$$

Eq. 52 clearly indicates that P is always zero if there is no thermal loading (i.e. $\Delta T = 0$), which means that Stage IV' does not exist when $\Delta T = 0$.

Load -displacement responses

According to the closed-form solution presented above, the entire load-displacement curve of an FRP-to-concrete bonded joint subjected to combined thermal and mechanical loadings can be obtained. Fig. 3c shows the load-displacement response of a typical bonded joint at reference temperature, in which the segments from OA, AB, BC and CD correspond to the elastic stage (Stage I), elastic-softening stage (Stage II), elastic-softening-debonding stage (Stage III) and softening-debonding stage (Stage IV), respectively. During the elastic stage, the pull load increases linearly with the displacement, followed by a nonlinear increase up to a peak value, which is reached at the slip value of δ_f. The ultimate load remains basically unchanged (i.e. reduces very slowly) during the elastic-softening-debonding stage for a range of displacement values if the bond length is sufficiently long. Afterwards, the load-displacement curve exhibits a descending part first and then a snapback part, which ends at a displacement value of δ_f.

Validation of the analytical solution

To verify the analytical solution, analytical predictions are compared in this section with the limited experimental results available in the literature (Klamer 2006, 2009). In addition, a simple FE model was developed to provide FE predictions to further demonstrate the validity of the analytical solution.

Klamer's tests

Klamer (2006, 2009) conducted a series of pull tests on double-lap FRP-to-concrete bonded joints (Fig. 4a) at temperatures ranging from -20 ^{o}C to 100 ^{o}C. The test specimens (including the installation of strain gauges on the FRP plate) were prepared at 20 ^{o}C (the reference temperature) but the tests were conducted at a different temperature (-20 ^{o}C, 20 ^{o}C, 40 ^{o}C, 50 ^{o}C, 70 ^{o}C, 80 ^{o}C or 100 ^{o}C). The thicknesses of the FRP pultruded plate and the adhesive layer were 1.2 mm and 1.5 mm, respectively, while the bond length was 300 mm. In making the predictions, the following geometric and material properties were used as provided by Klamer (2006): b_p = 100 mm, t_c = 75 mm, b_c = 150 mm, E_p = 165 000 MPa, E_c = 26 800 MPa, α_c = 10.2×10^{-6}/^{o}C and α_P = 0.3×10^{-6}/^{o}C. From the experimental load-displacement curves of the two specimens tested at reference temperature (20 ^{o}C), the load and slip values corresponding to the initiation of softening were identified (i.e. defined based on inspection) to be 20 kN and 0.09 mm, respectively. The ultimate load was averaged from the two test values to be 45.92 kN and hence the interfacial fracture energy was found to

be 0.57 N/mm (Yuan et al. 2004). The other two parameters of the bond-slip curve, namely δ_f and τ_f, were identified by least square analysis to obtain a best-fit curve for the combined data of the two test load-displacement curves. The results turned out to be: δ_f= 0.41 mm and τ_f= 2.77 MPa. Fig. 4b shows a comparison between the two test load-displacement curves and the corresponding curve predicted using the analytical solution of Yuan et al. (2004) (which is a special case of the present solution) and based on the identified bond-slip curve, indicating that the identified bond-slip curve leads to close predictions of the test results.

Comparisons with test results of Klamer (2006)

Fig. 5a presents a comparison between the predicted thermal strains in the CFRP plate and the experimental values for one of the specimens which was subjected to a temperature increase of 30 ^{o}C (i.e. ΔT= 30 ^{o}C) before the mechanical load was applied [Klamer (2006) reported the thermal strains of the FRP plate only for this specimen]. The close agreement between the test results and the analytical predictions demonstrates the validity of the present closed-form solution when only the thermal loading is considered.

Fig. 5b shows a comparison between the ultimate loads of FRP-to-concrete bonded joints obtained from Klamer's (2006) tests and the analytical solution. In this figure, the ultimate loads are normalized by the corresponding (experimental or predicted) value for the reference temperature of 20 ^{o}C for a clearer comparison. It is seen that the experimental ultimate load initially increases as the temperature increases (or decreases as the temperature reduces) but the trend reverses when the temperature is around the glass transition temperature T_g of the bonding adhesive which was 62 ^{o}C (Klamer 2006). As shown in Fig. 5b, the analytical ultimate load increases monotonically with the temperature. The difference between the experimental ultimate load and the analytical prediction for temperatures above the glass transition temperature is due to the omission of the effect of softening of the bonding adhesive: in the present predictions, the bilinear bond-slip law was identified from the test results for the reference temperature of 20 ^{o}C. In addition, any softening of the adherends was also ignored. The reasonably close agreement between the experimental results and the analytical predictions for temperatures below T_g further verify the reliability of the closed-form solution.

Comparisons with FE predictions

In the FE model (Fig. 6), two-node truss elements are used to represent the FRP plate and the concrete prism in accordance with the assumption adopted for the analytical solution that both adherends experience only membrane deformation. The bond-slip behavior between the two adherends is modeled using zero-thickness cohesive elements. All nodes of the bottom surface of the concrete prism are restrained against vertical movement and the node at the bottom right corner is additionally restrained against horizontal displacement. The FE model was implemented with ABAQUS (2008) and the well-known arc-length method was employed to trace the full-range load-displacement response that involves the snapback phenomenon.

In the analytical solution, it is assumed that the bond-slip response is fully reversible when slip reversals occur (Fig. 7a). In the FE model, a more realistic assumption for the effect of slip reversal can also be used: the bond resistance is no longer recoverable once the

interfacial slip has exceeded δ_f (Fig. 7b); the softening part of the bond-slip curve is still assumed to be fully recoverable. The use of the bond-slip model of Fig. 7b in the analytical solution would create difficulty for the derivation of a closed-form solution.

Fig. 8a presents load-displacement curves of bonded joints for different temperature variations predicted by both the analytical solution and the FE model using geometric and material properties (including the identified bond-slip curve) of Klamer's (2006) two reference test specimens. The bond-slip response of Fig. 7a was used in both approaches for obtaining the results shown in Fig. 8a. Obviously, the two approaches lead to identical results, confirming the validity and accuracy of both approaches.

In Fig. 8b, FE predictions based on the two different bond-slip laws of Fig. 7a and Fig. 7b are compared. Only a small difference between the two bond-slip laws is seen during the softening-debonding stage for $\Delta T > 0$ while no difference is seen for $\Delta T < 0$. Results obtained based on the linear damage model of Fig. 7c, if shown in Fig. 8b, are indistinguishable from those based on Fig. 7b and are thus not included in Fig. 8b. Similar to Fig. 3c, the segments of OA, AB, BC and CD in Fig. 8b correspond to the elastic, elastic-softening, elastic-softening-debonding and softening-debonding stages, respectively. If $\Delta T > 0$, the softening-debonding stage CD can be further divided into two sub-stages, CC' and $C'D$ (Stage VI'), as explained earlier. At point O, an initial displacement exists due to the thermal action. This displacement has usually been ignored in previous studies when interpreting the test results of FRP-to-concrete bonded joints subjected to a positive or negative temperature change (Klamer 2006; Leone et al. 2009), which is inappropriate. The snapback portion ends at a displacement value of δ_f when $\Delta T \geq 0$ but at a larger value when $\Delta T < 0$; this is because the debonded part of the interface cannot be reloaded in the case of $\Delta T < 0$ as discussed previously.

Fig. 9 presents numerical results from the analytical solution to examine the effect of temperature variation on the normalized ultimate load for FRP plates of different thicknesses (i.e. different tensile stiffnesses), with ΔT = 0 ^{o}C being for the reference case. It is clearly seen that for the same temperature rise, the increase in the ultimate load is larger when a thicker FRP plate is used. If a 2.4 mm thick FRP plate is used, a temperature decrease of 50 ^{o}C (e.g. from an installation temperature of 25 ^{o}C to a winter temperature of -25 ^{o}C) leads to approximately a 26% decrease in the ultimate load. This detrimental effect of temperature decrease on bond resistance needs to be properly considered in engineering practice when an FRP-strengthened structure is subjected to significant service temperature variations.

Response of the FRP-to-concrete interface

Interfacial shear stress and slip distributions at various deformation states of bonded joints exposed to a positive and a negative temperature variation are illustrated in Figs.10 and 11 respectively. In these figures, analytical predictions for characteristic deformation states are represented using continuous or dashed lines while a dotted line is used to represent an intermediate deformation state to illustrate the evolution of stresses and slips. Note that these results were obtained for plate and concrete material properties from Klamer's tests (2006) and the same bond-slip parameters as described in Section 3.1. In addition, FE predictions are shown as hollow circles only for the intermediate deformation state to confirm the agreement

between analytical and FE predictions. The focus of the discussions in the remainder of this section is on the effect of temperature variation on interfacial behaviour.

Bonded joint exposed to a temperature increase

Fig. 10 shows how the interfacial shear stress distribution and the interfacial slip distribution vary as deformation progresses for a temperature increase of 30°C (i.e. ΔT =30°C and T =50°C) in comparison with corresponding results for the reference temperature of 20°C. When only the thermal loading is applied (point O in Fig. 8b), both the interfacial shear stress and the slip due to a temperature increase are anti-symmetrically distributed, with the slip at the load end being negative. The interfacial shear stresses and slips from the pull load are opposite in direction to those from the thermal loading, so the two types of load lead to interfacial shear stresses and slips that counteract each other. That is, part of the pull load in a bonded joint exposed to a temperature increase is resisted by the thermal stresses and as a result, a temperature increase leads to an increase in the load levels of all characteristic deformation states except the completely unloaded state when the pull load is reduced back to zero (Fig. 8b). The phenomenon of an increase in the ultimate load due to a temperature increase has previously been discussed by Rabinovitch (2010) who correctly attributed the phenomenon to counteracting interfacial stresses.

Once the interfacial shear stress at the loaded end reaches its maximum value τ_f (with a corresponding slip of δ_1) (point A in Fig. 8b), the FRP-to-concrete interface enters the elastic-softening stage (segment AB in Fig. 8b), as described in Fig. 10b. Afterwards, debonding initiates first at the loaded end (point B in Fig. 8 b) and then propagates along the bond length until the slip at the free end reaches δ_1 (point C in Fig. 8c), as illustrated in Fig. 10c. Figs. 10b and 10c show that a positive temperature variation leads to a slightly longer length for the softening zone and a slightly shorter length for the debonded zone than those for the reference temperature. Furthermore, Fig. 10d shows that the softening zone expands towards the loaded end in the unloading stage (segment CD in Fig. 8b); this expansion is due to reductions of slip values to below δ_f coupled with the assumption of a fully reversible bond-slip law (Fig. 7a) which allows the debonded part of the bond length to regain bond resistance.

When the interfacial shear stress at the free end reduces to zero, the slip values of the entire interface are equal to δ_f for a bonded joint not exposed to a temperature variation (Fig. 10d), which signifies complete debonding of the entire interface. However, the situation is different for a bonded joint exposed to a temperature increase: when the interfacial shear stress at the free end reduces to zero, the interface enters the second sub-stage (Stage VI') of the soft-debonding stage as represented by segment C'D in Fig. 8b; debonding starts at the free end and propagates towards the loaded end until the whole interface is fully separated (Fig. 10e). At the end of debonding, the slip at the loaded end equals to δ_f while the slip values at other locations are greater than δ_f by an amount due to thermal expansion (Fig. 10e).

Bonded joint exposed to a temperature decrease

Similar to Fig. 10, the response of a bonded joint exposed to a temperature decrease of 30°C (i.e. ΔT = -30°C and T = -10°C) is examined in Fig. 11; the results for the reference

temperature case are again shown for comparison. Naturally, a temperature decrease alone leads to interfacial shear stresses and slips that are opposite in direction to those due to a temperature increase of the same magnitude (Fig. 11a), and this means that the pull load leads to interfacial shear stresses and slips in the same direction as the thermal loading in the zone near the loaded end. These thermal stresses are detrimental to the ultimate load and reduce the load values of the characteristic deformation states (Fig. 8b). A temperature decrease is seen to lead to a slightly shorter softening zone and a slightly longer debonding zone (Figs 11b and 11c). Unlike a bonded joint exposed to a temperature increase (Figs. 10d-10e), the slip values along the entire interface of a bonded joint exposed to a temperature reduction increase monotonically during the first three deformation stages (Figs. 11a-11c). During the softening-debonding stage (Fig. 11d), slip reversals occur but these reversals are never large enough to reduce a slip value larger than δ_f to below δ_f; that is, the assumption of a fully reversible bond-slip law has no consequence. At the end of debonding, the slip value at the free end reaches δ_f while the slip values elsewhere are all greater than δ_f, indicating the end of debonding.

Determination of interfacial fracture energy from pull tests

It is now clear that the ultimate load of an FRP-to-concrete bonded joint can be significantly affected by a temperature variation from the reference temperature (i.e. the installation temperature). This has a significant implication when pull test results are used to derive bond-slip curves. In such a derivation, the interfacial fracture energy G_f is directly related to the ultimate load of the bonded joint when temperature variations are not involved (e.g. Wu et al. 2002; Dai and Ueda. 2003; Lu et al. 2005a). When pull tests are used to derive bond-slip laws at a temperature variation, previous authors have followed the same approach (Wu et al. 2005). In the correct approach, the effect of thermal stresses on the ultimate load needs to be eliminated and the revised ultimate load can then be used to determine the interfacial fracture energy for the establishment of the bond-slip curve which may include the effect of softening of the bonding adhesive. That is, the interfacial fracture energy at temperature T is related to the experimental ultimate load $P_{u,T}$ by the following equation:

$$G_{f,T} = \frac{\left\{P_{u,T} + \frac{\tau_f b_p}{\lambda_1^2 \delta_1}(\alpha_p - \alpha_c)\Delta T \cdot \left[1 - \frac{\cos(\lambda_2 a_d)}{\cosh\left(\lambda_1 (L - a_d)\right)}\right]\right\}^2}{2 b_p^2 E_p t_p} \tag{54}$$

The problem with the above equation is that a_d is implicitly defined by Eq. 35 and can only be found by iterations. However it can be shown that for a sufficiently long bond length L and with the simplification that $\cosh\left(\lambda_1 (L - a_d)\right)$ is infinite, Eq. 54 reduces to

$$G_{f,T} = \frac{\left[P_{u,T} + \frac{\tau_f b_p}{\lambda_1^2 \delta_1}(\alpha_p - \alpha_c)\Delta T \cdot\right]^2}{2 b_p^2 E_p t_p} \tag{55}$$

If the test involves softening of the adherends as well, the above equations can still be used provided that the thermally induced deteriorations of material properties of the adherends are properly considered, such as using the model proposed by Dai et al. (2010) for FRP plates at elevated temperatures.

Conclusions

This paper has presented a closed-form analytical solution for the full-range behavior of FRP-to-concrete bonded joints under combined thermal and mechanical loadings. A bilinear local bond-slip relationship is employed in the solution, but the general characteristics observed from the solution are applicable to interfaces with a similar bond-slip model. The solution provides closed-form expressions for the interfacial slip, the interfacial shear stress, the axial stress in the FRP plate as well as the load-displacement response for the entire deformation process. The predictions of the closed-form solution have been compared with the existing test data available and finite element results, demonstrating close agreement between results from the three different approaches. It has been shown that, provided the material properties are not affected by temperature variations, a temperature rise increases the ultimate load while a temperature reduction decreases the ultimate load; the latter can have serious implications for the safety of the strengthened structure. A useful function of the closed-form solution lies in the interpretation of pull test results: the solution allows the effect of thermal stresses to be isolated from the effect of property changes of the bondline in obtaining bond-slip responses from pull tests.

It is worth noting that while the solution is developed with particular reference to FRP-to-concrete bonded joints, it is also applicable to similar bonded joints made of other materials (e.g. FRP-to-steel bonded joints) where the interfacial bond-slip law can be approximated as bi-linear. Furthermore, the solution can also be applied to situations where differential expansions between the two adherends are induced by factors other than thermal loading (e.g. moisture-induced differential expansions).

Acknowledgements

The authors are grateful for the financial support received from the Research Grants Council of the Hong Kong SAR (Project No: PolyU 516509) and for a PhD studentship awarded to the first author by The Hong Kong Polytechnic University.

References

ABAQUS. (2008). *ABAQUS standard user's manual,* Volumes I-III, Version 6.8. Hibbitt, Karlsson & Sorensen, Inc., Pawtucket, America.

Achintha, P.M.M. (2009). "Fracture analysis of debonding mechanism for FRP plates." PhD thesis, University of Cambridge, UK.

Blontrock, H. (2003). "Analysis and modeling of the fire resistance of concrete elements with externally bonded FRP reinforcement." PhD thesis, Ghent University, Belgium.

Brosens, K. (2001). "Anchoring of externally bonded steel plates and CFRP laminates for the strengthening of concrete elements." PhD thesis, Katholieke University Leuven, Belgium.

Chajes, M.J., Finch, W.W., Januszuka, T.F. and Thomson, T.A. (1996). "Bond and force transfer of composite material plates bonded to concrete." *ACI Structural Journal*, Vol. 93, No. 2, pp. 208-217.

Chen, J.F. and Teng, J.G. (2001). "Anchorage strength models for FRP and steel plates bonded to concrete." *Journal of Structural Engineering*, ASCE, Vol. 127, No. 7, pp. 784-791.

Chen, J.F., Yuan, H., and Teng, J.G. (2007). "Debonding failure along a softening FRP-to-concrete interface between two adjacent cracks in concrete members." *Engineering Structures*, Vol. 29, No. 2, pp. 259-270.

Cornetti, P. and Carpinteri, A. (2011). "Modeling the FRP-concrete delamination by means of an exponential softening law." *Engineering Structures*, Vol. 33, No. 6, pp. 1998-2001.

Dai, J.G., and Ueda, T. (2003). "Local bond stress slip relationship for FRP composites-concrete interfaces." *Proceedings of the Sixth International Symposium on FRP Reinforcement for Concrete Structures (FRPRCS-6)*, Singapore, pp. 143-152.

Dai, J.G., Ueda, T., and Sato, Y. (2005). "Development of the nonlinear bond stress-slip model of fiber reinforced plastics sheet-concrete interfaces with a simple method." *Journal of Composites for Construction*, ASCE, Vol. 9, No. 1, pp. 52-62.

Dai, J.G., Ueda, T. and Sato, Y. (2006). "Unified analytical approaches for determining shear bond characteristics of FRP-concrete interfaces through pullout tests." *Journal of Advanced Concrete Technology*, JSCE, Vol. 4, No. 1, pp. 133-145.

Dai, J.G., Gao, W.Y., and Teng, J.G. (2010). "Finite element modeling of reinforced concrete beams exposed to fire." *Proceedings of the Fifth International Conference on FRP Composites in Civil Engineering (CICE-2010)*, Beijing, China, pp. 428-432.

De Lorenzis, L., Miller, B., and Nanni, A. (2001). "Bond of fiber-reinforced polymer laminates to concrete." *ACI Material Journal*, Vol. 98, No. 1, pp. 256-264.

Ferracuti, B., Savoia, M. and Mazzotti, C. (2007). "Interface law for FRP-concrete delamination." *Composite Structures*, Vol. 80, No. 4, pp. 523-531.

Hollaway, L.C. and Teng, J.G. (2008). *Strengthening and Rehabilitation of Civil Infrastructures Using FRP* Composites. Woodhead Publishing Limited, Cambridge, UK.

Klamer, E. (2006). "The influence of temperature on concrete structures strengthened with externally bonded CFRP." Research Report, Eindhoven University of Technology, Netherlands.

Klamer, E. (2009). "Influence of temperature on concrete beams strengthened in flexure with CFRP." PhD Thesis, Eindhoven University of Technology, Netherlands.

Leone, M., Matthys, S., and Aiello, M.A. (2009). "Effect of elevated service temperature on bond between FRP EBR systems and concrete." *Composites Part B: Engineering*, Vol. 40, No. 1, pp.85-93.

Lu, X.Z., Teng, J.G., Ye, L.P. and Jiang, J.J. (2005a). "Bond-slip models for FRP sheets/plates bonded to concrete." *Engineering Structures*, Vol. 27, No. 6, pp. 920-937.

Lu, X.Z., Ye, L.P., Teng, J.G. and Jiang, J.J. (2005b). "Meso-scale finite element model for FRP sheets/plates bonded to concrete." E*ngineering Structures*, Vol. 27, No. 4, pp. 564-575.

Nakaba, K., Kanakubo, T., Furuta, T., and Yoshizawa, H. (2001). "Bond behavior between fiber-reinforced

polymer laminate and concrete." *ACI Structural Journal*, Vol. 98, No. 3, pp. 359-367.

Rabinovitch, O. (2010). "Impact of thermal loads on interfacial debonding in FRP strengthened beams." *International Journal of Solids and Structures*, Vol. 47, No. 24, pp. 3234-3244.

Taljsten, B. (1996). "Strengthening of concrete prisms using the plate-bonding technique." *International Journal of Fracture*, Vol. 82, No. 3, pp. 253-266.

Teng, J.G., Chen, J.F., Smith, S.T. and Lam, L. (2002). *FRP-Strengthened RC Structures*. John Wiley and Sons Ltd., Chichester, UK.

Teng, J.G., Yuan, H., and Chen, J.F., (2006). "FRP-to-concrete interface between two adjacent cracks: Theoretical model for debonding failure." *International Journal of Solid and Structures*, Vol. 43, Nos 18-19, pp. 5750-5778.

Wang, J. (2007). "Cohesive-bridging zone model for FRP-concrete interface debonding." *Engineering Fracture Mechanics*, Vol. 74, No. 17, pp. 2643-2658.

Wu, Z.S., Yuan, H. and Niu, H. (2002). "Stress transfer and fracture propagation in different kinds of adhesive joints." *Journal of Engineering Mechanics*, ASCE, Vol. 128, No. 5, pp. 562-573.

Wu, Z.S., Iwashita, K., Yagashiro, S., Ishikawa, T., and Hamaguchi, Y. (2005). "Temperature effect on bonding and debonding behavior between FRP sheets and concrete." *Journal of the Society of Materials Science*, Vol. 54, No. 5, pp. 474-480.

Yao, J., Teng, J.G., and Chen, J.F. (2005). "Experimental study on FRP-to-concrete bonded joints." *Composites Part B: Engineering*, Vol. 36, No. 2, pp. 99-113.

Yuan, H., Wu, Z.S. and Yoshizawa, H. (2000). "Theoretical solutions on interfacial stress transfer of externally bonded steel/composite laminates." *Journal of Structural Mechanics and Earthquake Engineering*, JSCE, Vol. 18, No. 1, pp. 27-39.

Yuan, H., Teng, J.G., Seracino, R., Wu, Z.S. and Yao, J. (2004). "Full-range behavior of FRP-to-concrete bonded joints." *Engineering Structures*, Vol. 26, No. 5, pp. 553-565.

Zhou, Y.W., Wu, Y.F. and Yun, Y. (2010). "Analytical modeling of the bond-slip relationship at FRP-concrete interfaces for adhesively-bonded joints." *Composites Part B: Engineering*, Vol. 41, No. 6, pp. 423-433.

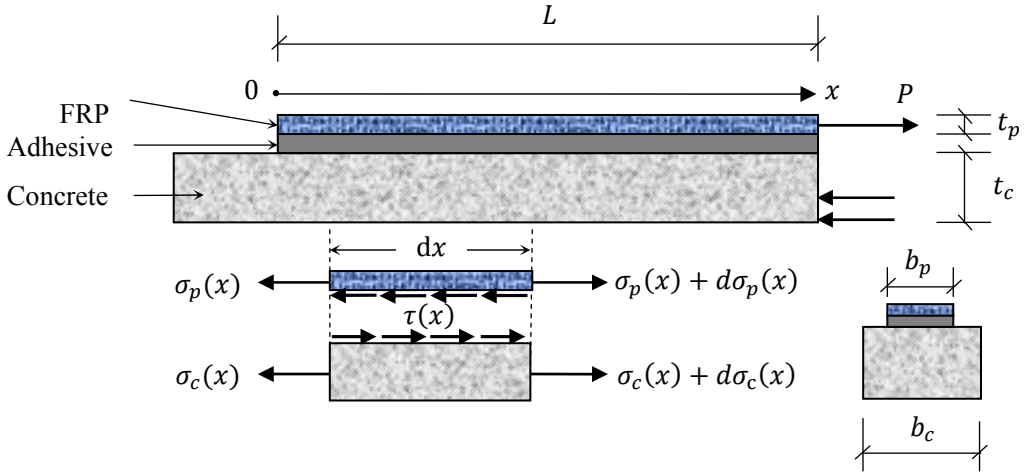

Fig. 1. Schematic diagram of a single-lap pull test.

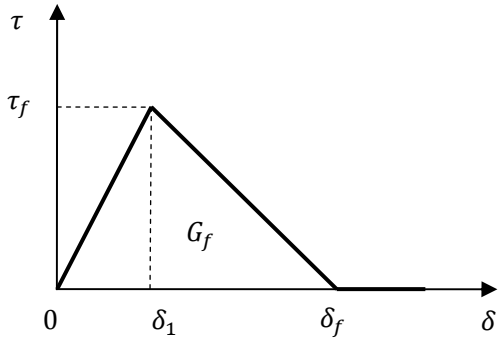

Fig. 2 Bi-linear bond-slip model.

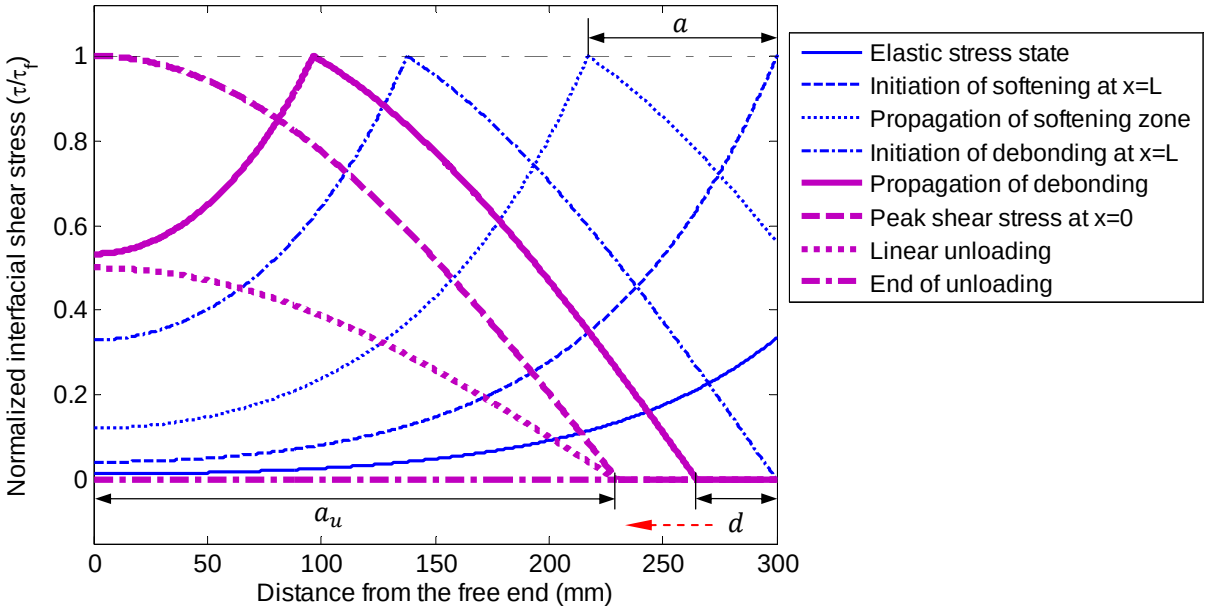

(a) Interfacial shear stress distribution

Fig. 3 Behavior of bonded joint at reference temperature.

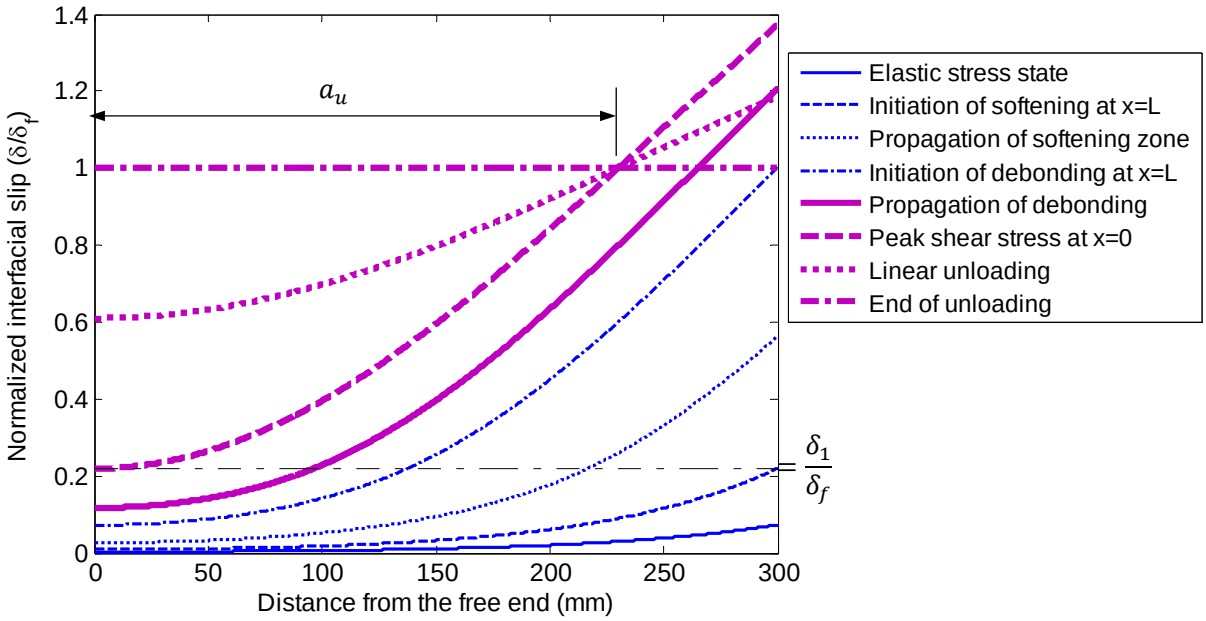

(b) Interfacial slip distribution

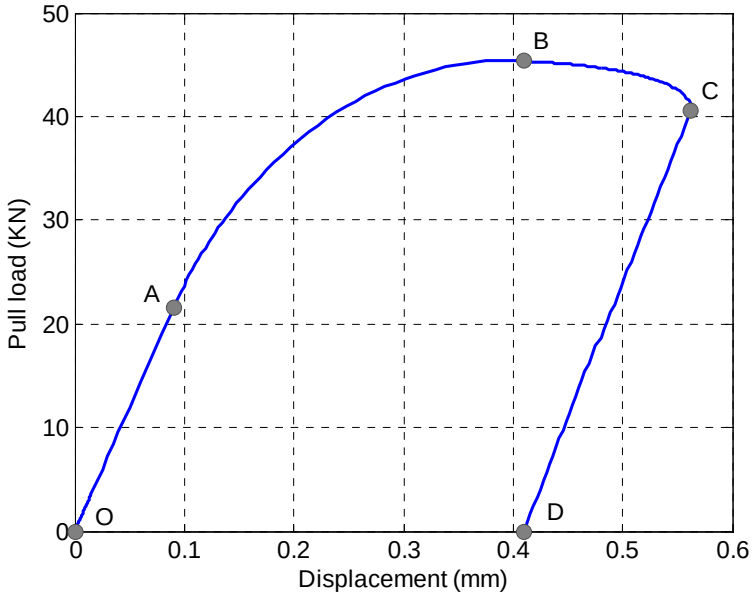

(c) Load-displacement response

Fig. 3 Behavior of bonded joint at reference temperature (Cont'd).

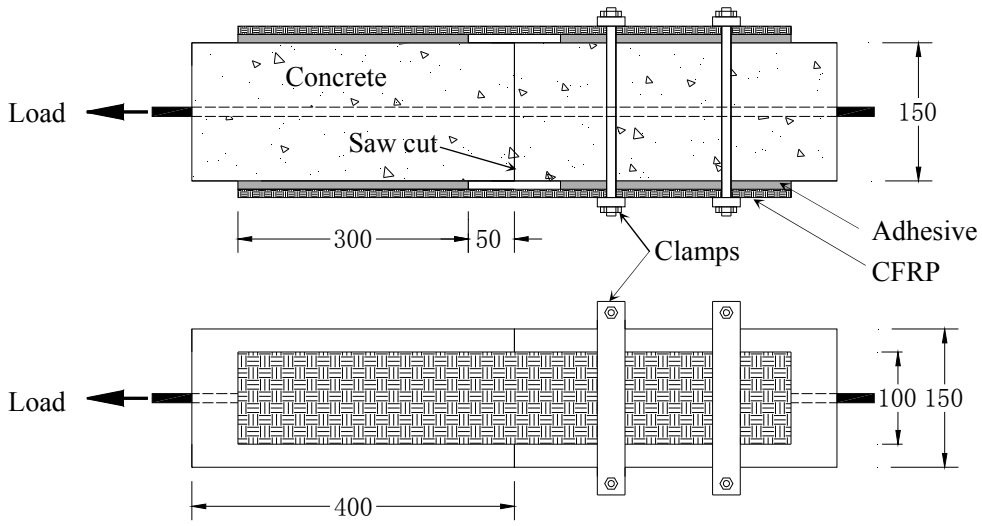

(a) Specimen details

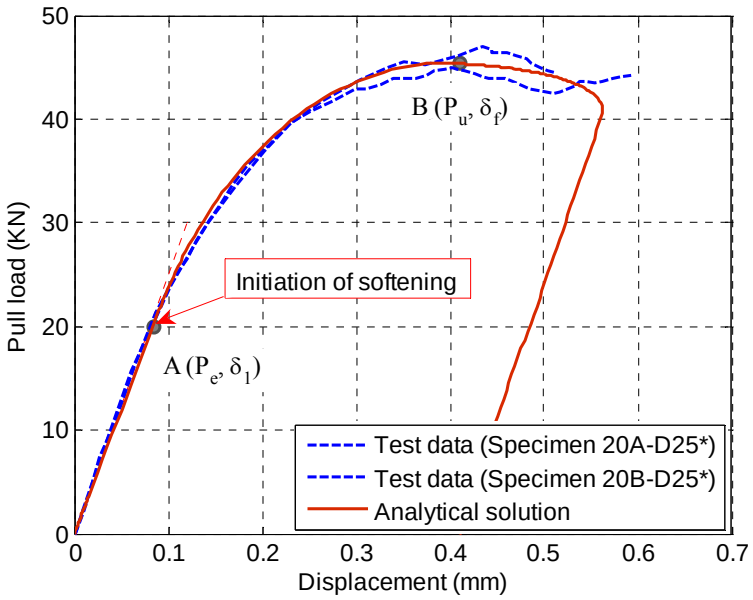

(b) Load-displacement curves

Fig. 4 Test specimens of Klamer (2006).

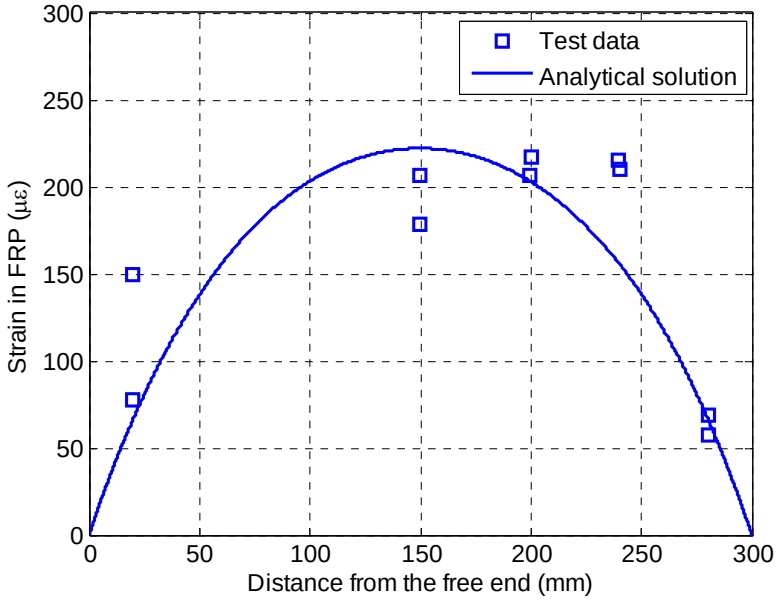

(a) Thermal strain distribution in the FRP.

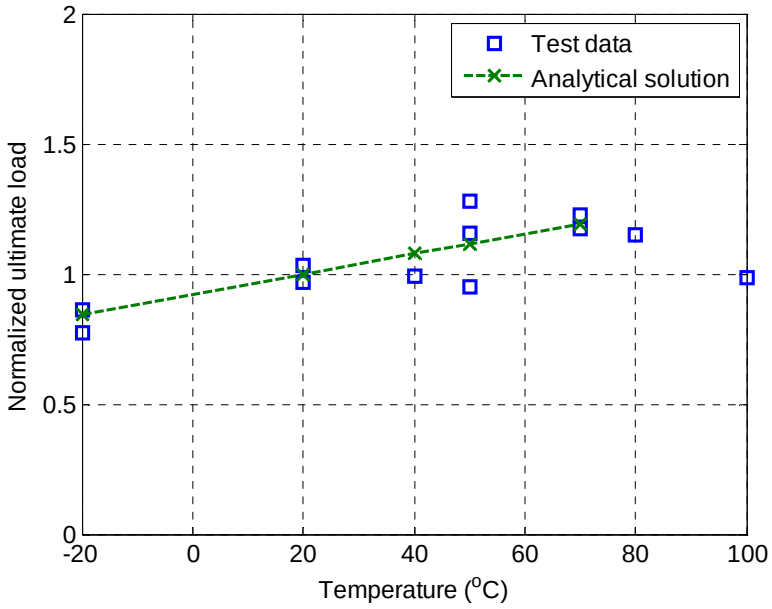

(b) Normalized ultimate load vs. temperature.

Fig. 5 Comparison with test results of Klamer (2006).

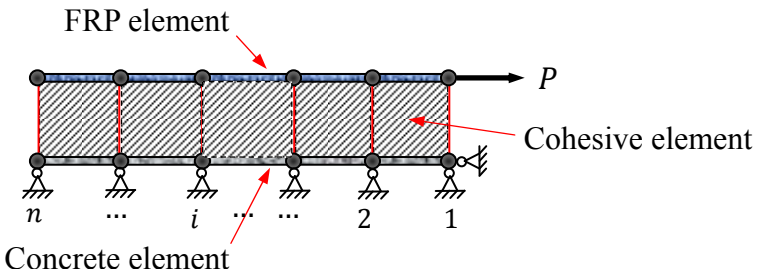

Fig. 6 Finite element model

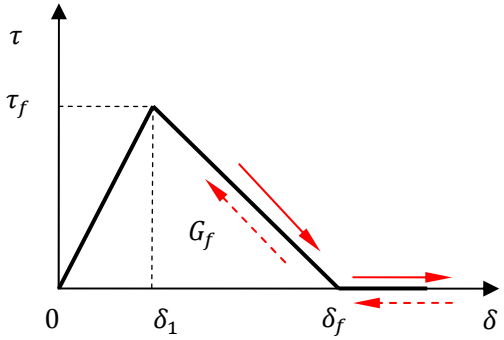

(a) Fully reversible

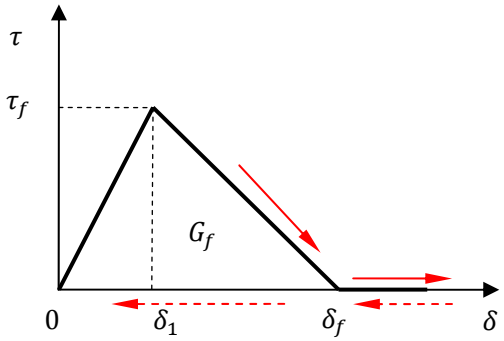

(b) Non-reversible after complete separation

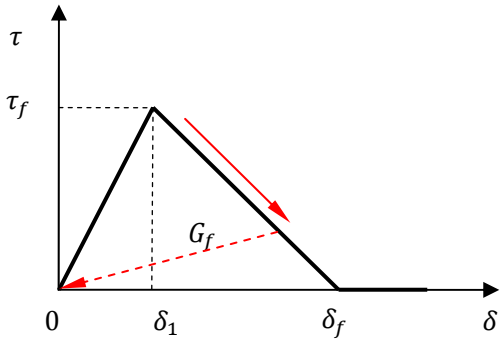

(c) Linear damage model

Fig. 7 Bond-slip responses during slip reversals.

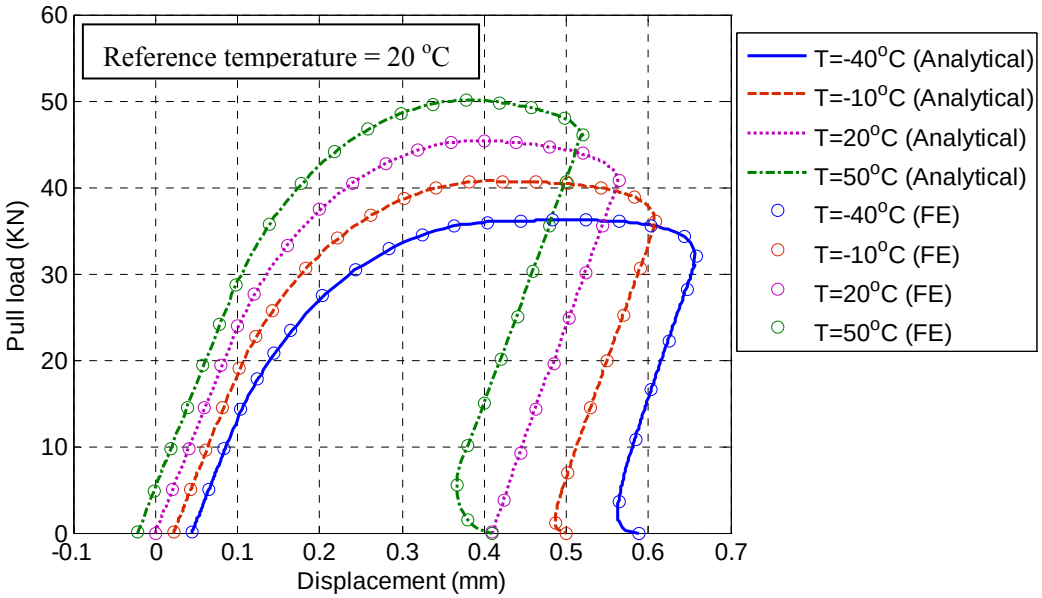

(a) Comparison between analytical and FE predictions.

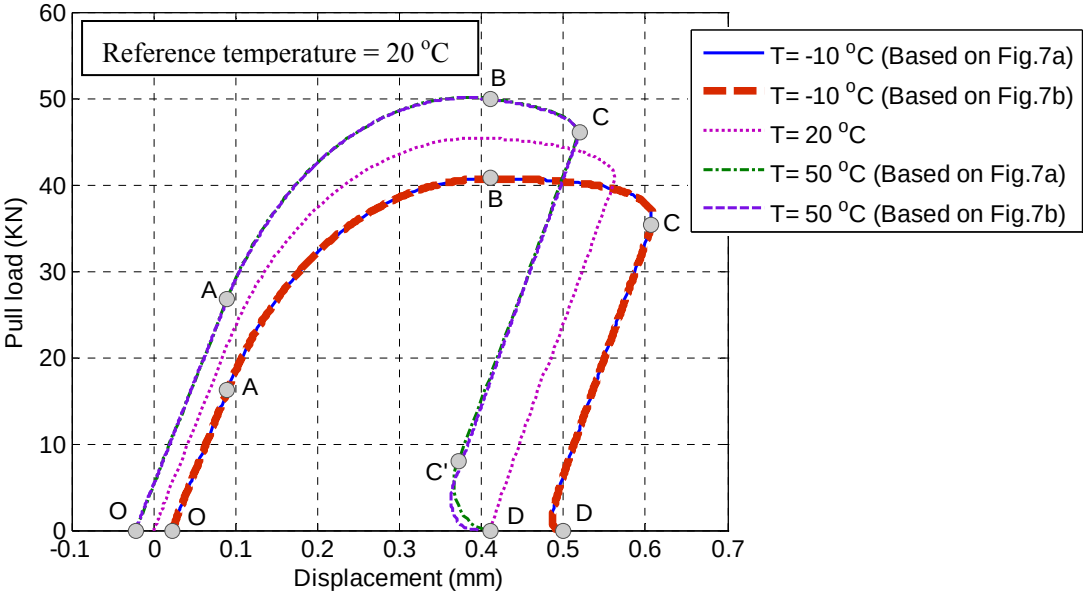

(b) Comparison between predictions based on different slip reversal responses.

Fig. 8 Effect of temperature variation on load-displacement response.

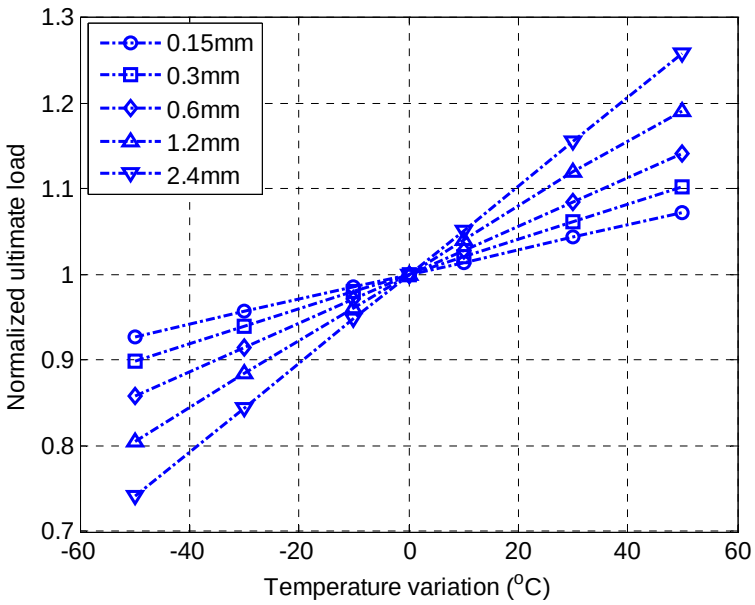

Fig. 9 Effect of temperature variation on ultimate load at different plate stiffness levels.

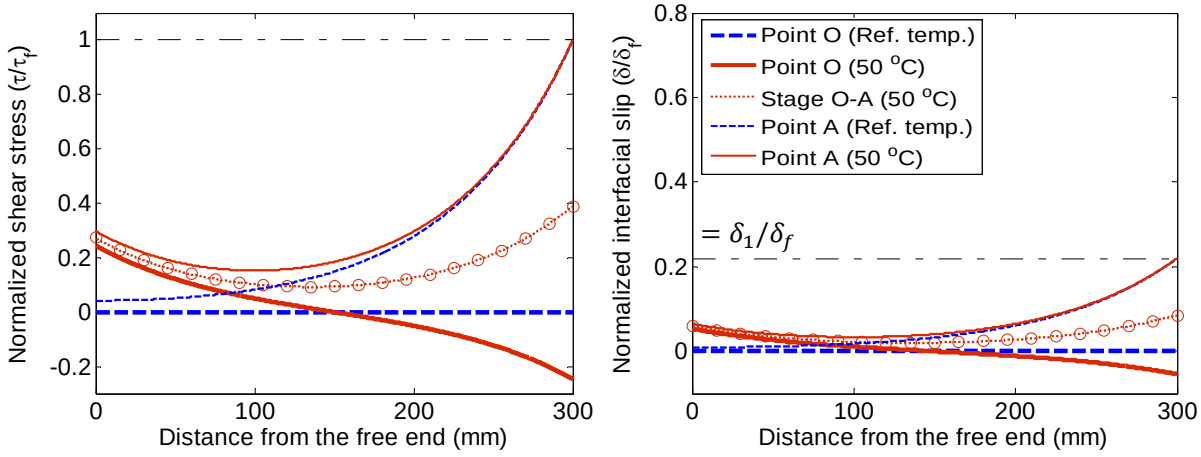

(a) Elastic stage (Stage I)

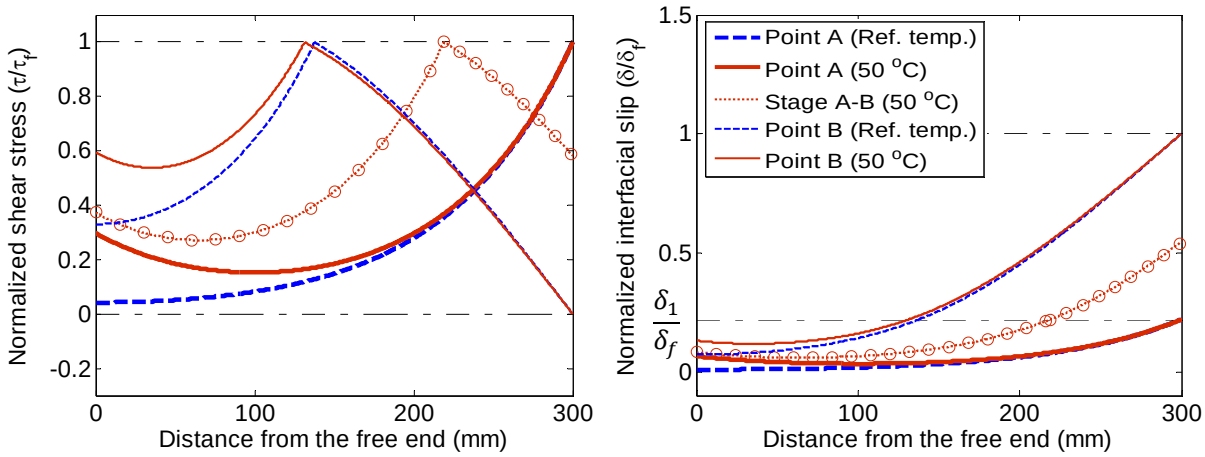

(b) Elastic-softening stage (Stage II)

Fig. 10 Bonded joint subjected to a temperature increase (ΔT = 30°C)

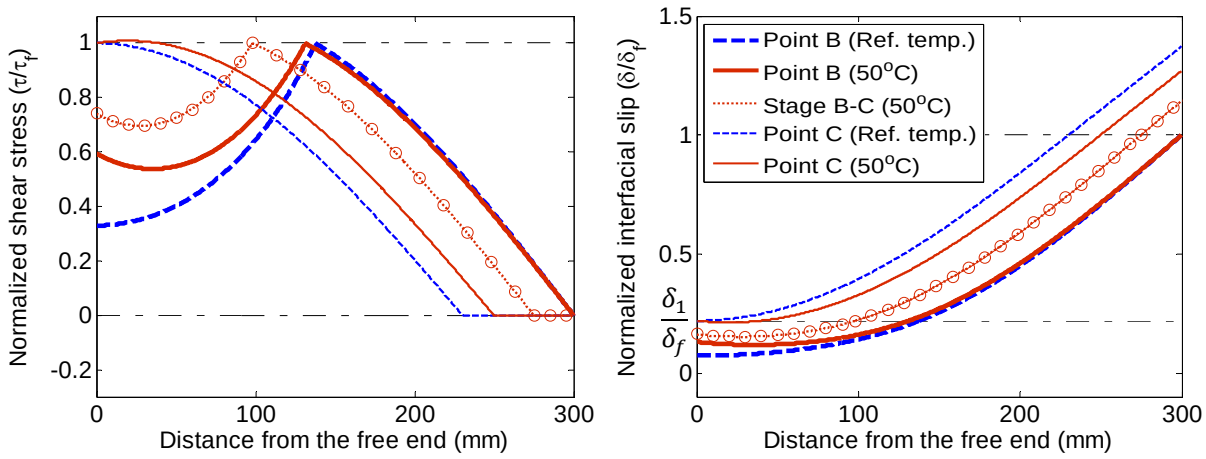

(c) Elastic-softening-debonding stage (Stage III)

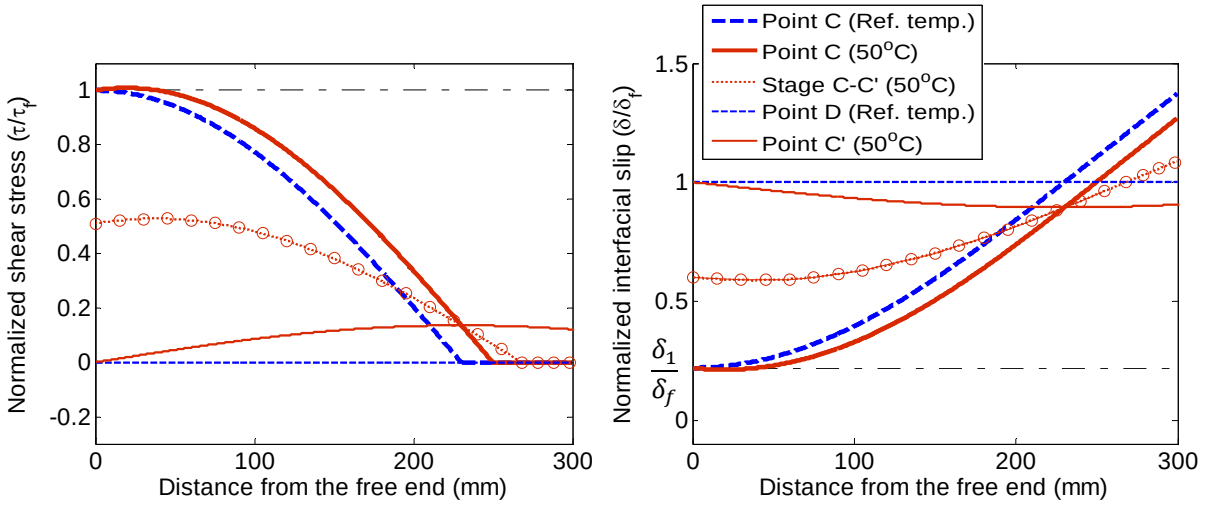

(d) Softening-debonding stage (Stage IV)

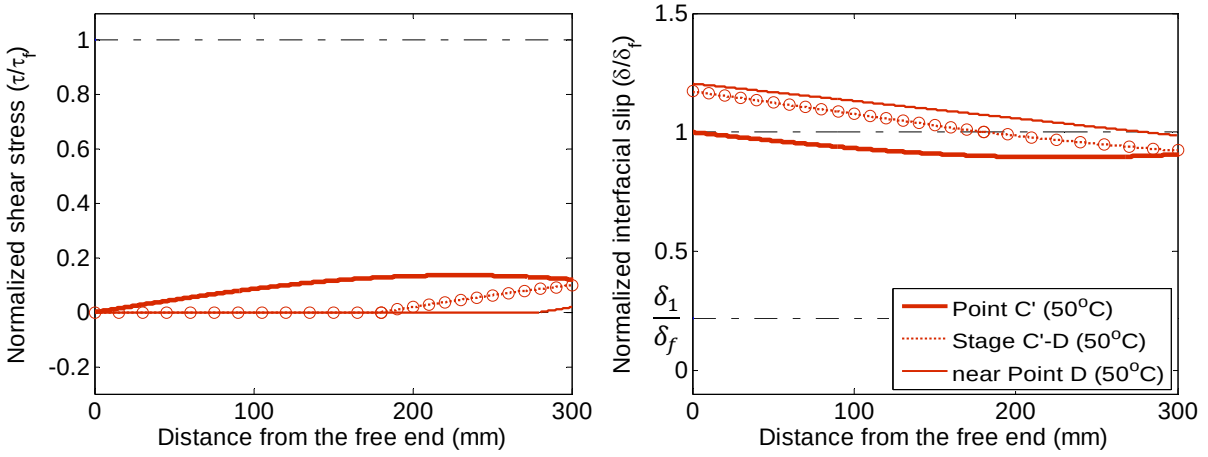

(e) Softening-debonding stage (Stage IV')

Fig. 10 Bonded joint subjected to a temperature increase (ΔT = 30°C) (Cont'd).

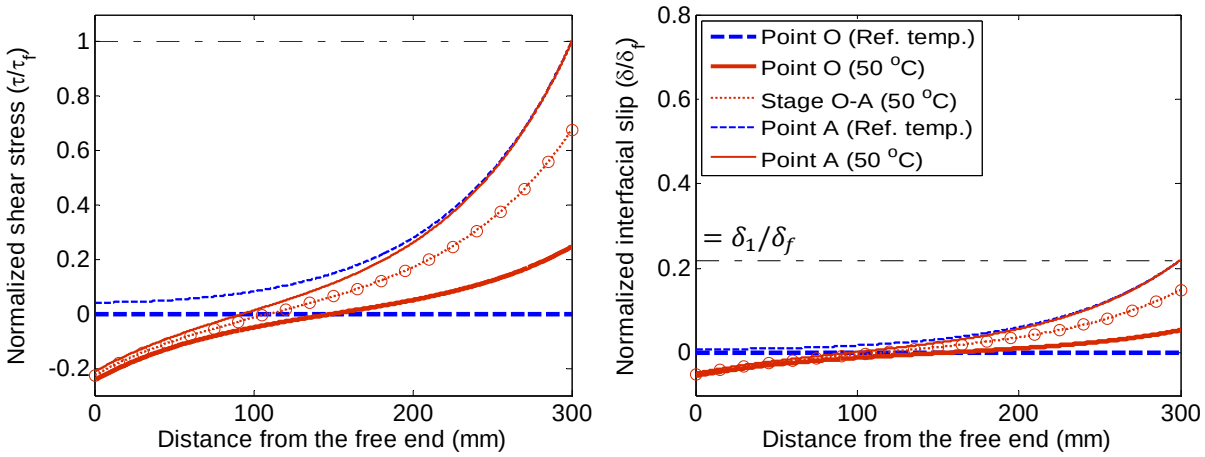

(a) Elastic stage (Stage I)

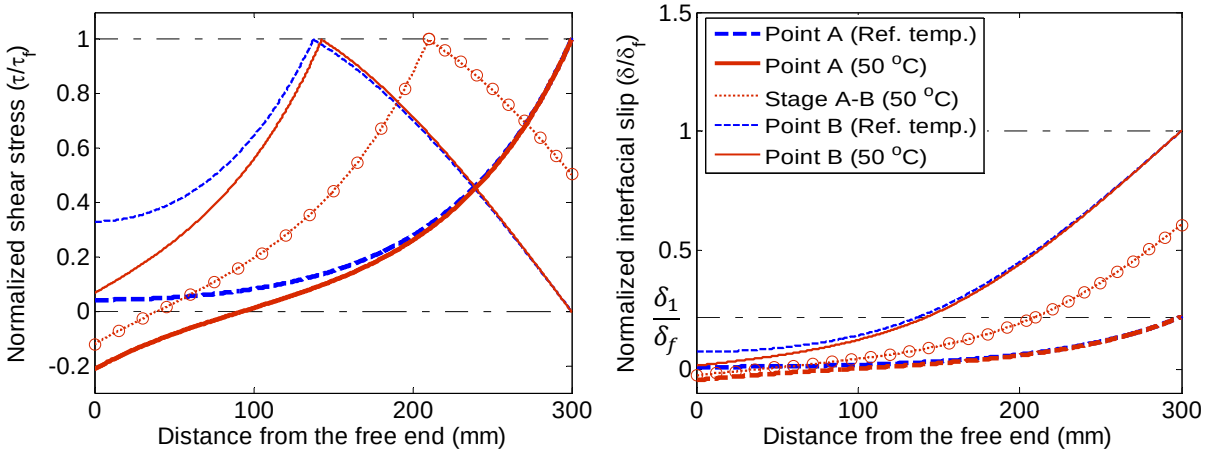

(b) Elastic-softening stage (Stage II)

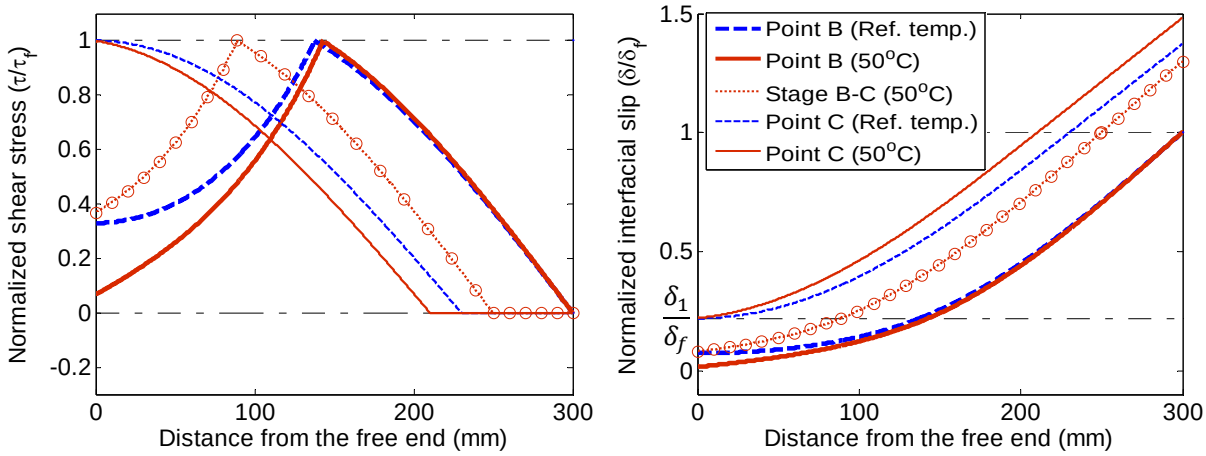

(c) Elastic-softening-debonding stage (Stage III)

Fig. 11 Bonded joint subjected to a temperature decrease (ΔT = -30°C)

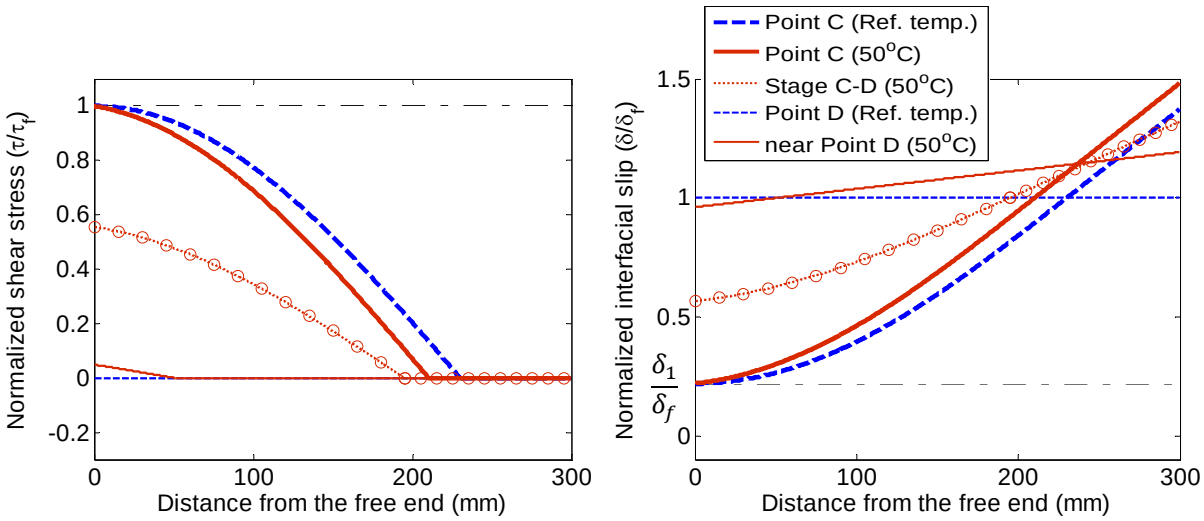

(d) Softening-debonding stage (Stage IV)

Fig. 11 Bonded joint subjected to a temperature decrease (ΔT = -30°C) (Cont'd).